Journal of Protein Chemistry, Vol. 18, No. 3, 1999

Correlation Between Self-Association Modes and GTPase Activation of Dynamin

Derk D. Binns,[1] Barbara Barylko,[1] Nikolai Grichine,[1] Mark A. L. Atkinson,[2] Michael K. Helms,[3] David M. Jameson,[3] John F. Eccleston,[4] and Joseph P. Albanesi[1,5]

Received December 4, 1998

The GTPase activity of dynamin is obligatorily coupled, by a mechanism yet unknown, to the internalization of clathrin-coated endocytic vesicles. Dynamin oligomerizes *in vitro* and *in vivo* and both its mechanical and enzymatic activities appear to be mediated by this self-assembly. In this study we demonstrate that dynamin is characterized by a tetramer/monomer equilibrium with an equilibrium constant of 1.67×10^{17} M^{-3}. Stopped-flow fluorescence experiments show that the association rate constant for 2′(3′)-O-N-methylanthraniloyl (mant)GTP is 7.0×10^{-5} M^{-1} s^{-1} and the dissociation rate constant is 2.1 s^{-1}, whereas the dissociation rate constant for mantdeoxyGDP is 93 s^{-1}. We also demonstrate the cooperativity of dynamin binding and GTPase activation on a microtubule lattice. Our results indicate that dynamin self-association is not a sufficient condition for the expression of maximal GTPase activity, which suggests that dynamin molecules must be in the proper conformation or orientation if they are to form an active oligomer.

KEY WORDS: Dynamin; self-association; GTPase activity; stopped-flow; mantGTP.

1. INTRODUCTION

Dynamin, a 100-kDa enzyme that catalyzes the hydrolysis of GTP,[6] plays an essential role in synaptic vesicle recycling (Chen *et al.*, 1991; van der Bliek and Meyerowitz, 1991; Takei *et al.*, 1995; McNiven, 1998) and in early steps of receptor-mediated endocytosis (Herskovits *et al.*, 1993*a*; van der Bliek *et al.*, 1993; Damke *et al.*, 1994; Urrutia *et al.*, 1997). Recent evidence (Sweitzer and Hinshaw, 1998; Takei *et al.*, 1998) supports the view that dynamin serves to constrict the necks of budding endocytic vesicles, although alternative roles for the enzyme have not been ruled out (Roos and Kelly, 1997). At least three forms of dynamin have been identified (Obar *et al.*, 1990; Chen *et al.*, 1991; Nakata *et al.*, 1993; Sontag *et al.*, 1994; Cook *et al.*, 1994), but only the brain-specific enzyme, dynamin I, has been purified to homogeneity and extensively characterized. Analysis of the dynamin I and II sequences reveals three structural domains. The N-terminal third of the molecule contains a tripartite GTP-binding domain characteristic of other GTP-binding proteins such as Ras (Obar *et al.*, 1990). The C-terminal half of the molecule has two modules implicated in protein–protein or protein–lipid interaction: a pleckstrin homology (PH) domain and a proline/arginine-rich domain (PRD) of about 100 amino acids extending to the C-terminus. The PRD contains several potential Src homology 3 (SH3)-binding motifs. Many SH3-containing proteins have been shown to interact with dynamin *in vitro* (Gout *et al.*, 1993; Herskovits

[1] Department of Pharmacology, U.T. Southwestern Medical Center, Dallas, Texas 75235–9041.
[2] Department of Biochemistry, U.T. Health Science Center, Tyler, Texas.
[3] Department of Genetics and Molecular Biology, University of Hawaii, Honolulu, Hawaii 96822.
[4] Division of Physical Biochemistry, National Institute for Medical Research, Mill Hill, London, NW7 1AA, United Kingdom.
[5] To whom correspondence should be addressed.

[6] Abbreviations: GTP, guanosine-5′-triphosphate; GTPase, guanosine-5′-triphosphatase; DTT, dithiothreitol; MES, 2-[N-morpholino] ethanesulfonic acid; PIPES, piperazine-N,N′-bis[2-2 ethanesulfonic acid]; PI(4,5)P_2, phosphatidylinositol 4,5-bisphosphate; SDS–PAGE, sodium dodecyl sulfate–polyacrylamide gel electrophoresis; BSA, bovine serum albumin; EGTA, ethylene glycol-bis(β-aminoethyl); GST, glutathione-S-transferase; Grb2, growth factor receptor binding protein 2; S, Svedbergs.

0277-8033/99/0300-0277$16.00/0

et al., 1993*b;* Seedorf *et al.,* 1994; Scaife *et al.,* 1994; Ando *et al.,* 1994; Miki *et al.,* 1994) and several (Grb2, Src, FGR, FYN) stimulate its GTPase activity (Gout *et al.,* 1993; Herskovits *et al.,* 1993*b*). Several other known *in vitro* activators of dynamin, i.e., microtubules and anionic liposomes, also bind to the PRD, possibly through charge interactions with basic residues within the dynamin tail (Herskovits, *et al.,* 1993*b*). These activators stimulate dynamin GTPase activity to a greater degree than do the SH3-containing proteins, with a maximal reported turnover of about 200 min^{-1} (Shpetner and Vallee, 1992; Maeda *et al.,* 1992; Tuma *et al.,* 1993; Tuma and Collins, 1994). Recently, we and others have reported that phosphoinositides can also potently stimulate dynamin GTPase activity, but in this case the lipids interact with the PH domain rather than with the PRD (Salim *et al.,* 1996; Lin *et al.,* 1997). Expression of dynamin GTPase activity is coupled to the oligomerization of dynamin, and microtubules and anionic liposomes may stimulate activity by providing a scaffold for dynamin self-assembly (Tuma *et al.,* 1993; Tuma and Collins, 1994). Moreover, self-association appears to be important for the cellular activity of dynamin since it occurs *in vivo;* dynamin polymers have been observed on clathrin-coated pits as they pinch off from the plasma membrane (Takei *et al.,* 1995).

The role of dynamin in clathrin-coated vesicle budding has been proposed to involve the following steps (Hinshaw and Schmid, 1995; De Camilli, 1995). Cytosolic dynamin, nucleotide-free or GDP-bound, gradually concentrates at regions of the plasma membrane where clathrin-coated pits are formed. Initially dynamin is diffusely distributed on the clathrin lattice, but upon GTP binding it rearranges into rings around the necks of invaginated coated pits. Hydrolysis of GTP induces conformational changes of dynamin, as yet unidentified, that result in constriction of the rings leading eventually to vesicle fission. After GTP hydrolysis, dynamin oligomers disassemble.

Several questions related to dynamin self-assembly remain to be answered. (1) What are the authentic docking proteins that promote dynamin self-assembly at the coated pit and how are their interactions with dynamin regulated? (2) What are the interaction sites between dynamin molecules? (3) Which steps of the GTPase catalytic pathway are affected by dynamin–dynamin interactions? *In vitro* studies show that many proteins are able to bind to dynamin, but the *in vivo* significance of these interactions is not yet clear. Recently, dynamin has been shown to interact directly with α-adaptins (Wang *et al.,* 1995) and with amphiphysin (David *et al.,* 1996), an SH3-containing protein enriched at the coated pit. However, no effect on GTPase activity by either α-adaptin or amphiphysin was reported. Microtubules are the most potent activators of dynamin GTPase activity, but their *in vivo* role has been questioned since dynamin does not codistribute with them in cultured cells (Scaife and Margolis, 1990) and microtubule-disrupting agents (e.g., nocodazole) do not affect the early steps of endocytosis. However, one group reported an 80% reduction in the rate of transferrin internalization in nocodazole-treated cells (Jin and Snider, 1993) and this effect could be explained by the involvement of membrane-bound tubulin in the budding of coated vesicles (Vallee and Okamoto, 1995). Tubulin is abundant in highly purified coated vesicles (Kelly *et al.,* 1993), though its status as a genuine coated vesicle component rather than a contaminant remains to be established. Whether or not tubulin determines dynamin self-assembly at the coated pit, it forms an optimal scaffold for dynamin oligomerization (see De Camilli, 1995). Therefore, it is likely that the information obtained by studying dynamin–microtubule interactions can be applied to *in vivo* situations.

In this study we focus on the relationship between GTPase activity and oligomerization of dynamin. We present evidence that dynamin self-association by itself is not sufficient to stimulate GTPase activity, suggesting that dynamin molecules in the oligomer must be in the appropriate conformation or orientation. Indeed, Muhlberg *et al.* (1997) have identified a site between the PH domain and the PRD which may be responsible for stimulation of the GTPase activity of one dynamin molecule by another. Our data suggest that ionic interactions are involved in aligning dynamin molecules on a surface to allow for maximal activation.

2. MATERIALS AND METHODS

2.1. Materials

Phosphocellulose P11 and diethylaminoethyl cellulose DE52 were from Whatman; SP-Sepharose and glutathione-Sepharose were from Pharmacia Biotech; protease inhibitors and GTP were from Sigma; [γ-^{32}P] GTP was from Amersham.

2.2. Purification of Proteins

2.2.1. Reagents

Fresh bovine brains were obtained from a local slaughterhouse, cooled on ice, and processed within 2 hr. All solutions used in the purification procedure contained

1 mM DTT, 1 mM sodium azide, and a range of protease inhibitors, namely 0.2 mM phenylmethylsulfonyl fluoride and 10 mg/L each of Nα-benzoyl-L-arginine methyl ester, Nα-*p*-tosyl-L-arginine methyl ester, Nα-*p*-tosyl-L-lysine chloromethyl ketone, leupeptin, and pepstatin A.

2.2.2. *Dynamin*

Dynamin I was purified from bovine brains essentially as described previously (Earnest *et al.,* 1996; Lin *et al.,* 1997). Brain tissue (about 500–700 g) was homogenized with 1–1.5 volumes of a solution containing 0.1 M MES, pH 7.0, 1 mM EGTA, 1 mM $MgSO_4$ 1 mM DTT, and protease inhibitors (buffer A). The homogenate was centrifuged at 30,000 × *g* and 4°C for 40 min, after which the supernatant solution was immediately loaded onto a DE52 cellulose column (6 × 10 cm) equilibrated with buffer A. The flowthrough was loaded directly onto a P11 phosphocellulose column (3 × 18 cm), also equilibrated with buffer A. The columns were extensively washed with buffer A, and then dynamin was eluted from the P11 column with buffer A containing 0.5 M NaCl. Eluted proteins were precipitated with 65% saturation ammonium sulfate and centrifuged at 30,000 × *g* for 20 min. The pellet was resuspended in buffer A and dialyzed extensively against the same buffer. The product was loaded onto a SP Sepharose column (3 × 18 cm) equilibrated with buffer A, and the column was washed with buffer A containing 0.05 M NaCl, then eluted with a 0.05–0.3 M NaCl linear gradient. Fractions containing dynamin were combined and dialyzed against buffer A. The sample was next incubated with taxol-stabilized microtubules for 15 min at 35°C and then centrifuged at 100,000 × *g* for 1 hr. To release dynamin from microtubules, the pellet was resuspended in a small volume (10–15 ml) of buffer A containing 10 mM GTP and the sample was centrifuged again at 100,000 × *g* for 1 hr. The supernatant was passed through a DE52 column to remove any traces of tubulin. At this stage, dynamin was usually about 90% pure. If necessary, dynamin was further purified on a 5–15% sucrose gradient centrifuged at 112,000 × *g* for 16 hr. GTP (final conc. 50 μM) was added to the dynamin solution and aliquots were quickly frozen in liquid nitrogen and stored at –70°C.

2.2.3. *Tubulin*

Tubulin was purified according to the procedure of Williams and Lee (1982) except that MES was used instead of PIPES buffer.

2.3. Analytical Procedures

2.3.1. *Binding Experiments*

Pelleting assays were used to measure the binding of dynamin to microtubules. Dynamin, either alone or mixed with taxol-polymerized tubulin, was incubated in buffer A containing additionally 10 μM taxol, 0.5 mg/ml BSA, and 1 mM Mg^{2+}-GTP for 15 min at 37°C, and then centrifuged at 140,000 × *g* for 10 min. The pellets were resuspended in a volume equal to the initial volume of the sample and the amount of dynamin in both the precipitate and supernatant solutions was determined by scanning SDS–polyacrylamide gels with a Molecular Dynamics scanner.

2.3.2. *GTPase Activities*

GTPase activities were measured by the release of $^{32}P_i$ from [γ-^{32}P]GTP (Korn *et al.,* 1982) after incubation at 37°C in the same solution as that used for binding experiments. The reaction time varied from 30 min for low dynamin concentrations to 1 min at high dynamin concentration to ensure that less than 15% of added GTP is hydrolyzed.

2.3.3. *Analytical Methods*

Protein concentrations were determined as described by Bradford (1976) using BSA as a standard. SDS–PAGE was carried out according to the method of Laemmli (1970) modified by Matsudaira and Burgess (1978).

2.3.4. *Analytical Ultracentrifugation*

All analytical ultracentrifugation experiments were performed in a Beckman XLA-Analytical Ultracentrifuge using absorbance optics in rotor An60Ti using a 12-mm double-sector centerpiece with a pathlength of 1.2 cm. For the sedimentation equilibrium run, the data were collected at 280 nm, 7000 rpm, and 4°C from cell radii of 6.8–7.2 cm, with a step size of 0.001 cm. Five readings were averaged for each scan in the final output. Successive scans were compared to determine if equilibrium had been reached. The loading concentration of dynamin was 0.33 mg/ml (determined by Bradford Assay) which had an initial absorbance of 0.280 at 280 nm. The experiment was performed in the following buffer: 20 mM HEPES, pH 7.0, 1.0 mM EDTA, 5 mM $MgCl_2$, 1 mM DTT, 300 mM NaCl, and 0.2 mM PMSF. The background absorbance was estimated by overspeeding at 40,000 rpm until a flat baseline was obtained. The overspeed absorbance

was 0.025. Data were analyzed using the program XLA-single (Beckman) using a molecular weight for bovine dynamin I of 100,000 Da. The models used were "ideall" (for single-species fits) and "assoc4" (which calculates monomer/ *n*-mer equilibrium constants for up to four interacting species). The program gives equilibrium constants in terms of absorbance units, and these were converted to concentration units using an extinction coefficient ε of 53,500 M^{-1} cm^{-1} (calculated for dynamins at 280 nm). The monomer/tetramer equilibrium constants were calculated using the following formula: $K_{1,4}$ (in units of M^{-3}) = $K_{1,4}$ [in units of $(abs)^{-3}$] $*$ $(1.2\ \varepsilon)^3/4$.

Sedimentation velocity data were collected at 280 nm, 20°C, and 35,000 rpm with a loading concentration of 0.325 mg/ml dynamin, which had an initial absorbance of 0.289. The data were collected from cell radii of 6.0–7.2 cm with a step size of 0.005 cm in the continuous mode. Five readings were averaged for each scan, and 15 scans were collected and analyzed. The data were analyzed using the second moment and $g(s^*)$ methods in XLA-veloc (Beckman). In the second-moment method, an equivalent boundary is calculated where the boundary would have been observed in the absence of diffusion. This boundary is calculated using the meniscus and plateau radii (where the concentration gradient is zero). A plot of ln(radius) versus $\omega^2 t$ (where ω is the angular velocity) is made, and the slope of the best fit line to this plot gives the weight-averaged sedimentation coefficient. In the $g(s^*)$ method (Stafford, 1992, 1994), an apparent sedimentation coefficient distribution function $g(s^*)$ is calculated. In this method, the difference of absorbance curves collected at successive times is first calculated. Each difference curve is then converted from a function of radius to a function of the sedimentation coefficient, and the difference curves are then averaged and used for the time derivative of the sedimentation velocity concentration curve. This time derivative is used to calculate $g(s^*)$ as a function of the sedimentation coefficient. This method gives a higher signal-to-noise ratio by removing time-independent effects in the baseline (Hensley, 1996). Since $g(s^*)$ represents a distribution function for sedimentation coefficients, the weight-averaged sedimentation coefficient can be calculated from the $g(s^*)$ curve using the relation

$$s_w = \sum[s(I)\,g(s(I))]/\sum[g(s(I))] \quad (1)$$

where s_w is a weight-averaged sedimentation coefficient, $s(I)$ is the sedimentation coefficient, and $g(s(I))$ is the value of the distribution function $g(s^*)$ at the particular value $s(I)$ (Stafford, 1994).

Frictional coefficients f were calculated from the sedimentation coefficient using the equation

$$f = M(1 - \upsilon\rho)/N_A s \quad (2)$$

where s is the sedimentation coefficient, M is the molecular weight, υ is the partial specific volume (see below), ρ is the solution density, and N_A is Avogadro's number. The radius of an equivalent sphere for a given frictional coefficient f was calculated using the equation

$$R = f/6\pi\eta \quad (3)$$

where η is the solvent viscosity and R is the radius of the equivalent sphere. The minimum radius of a sphere for a protein of a given molecular weight was calculated from

$$R^3_{\min} = M\upsilon/N_A\pi\,(4/3) \quad (4)$$

where the symbols are defined as above. The partial specific volume for dynamin I was 0.73 ml/g, as calculated by the method of Cohn and Edsall (1943), a method which has generally been found to give the most reliable molecular weights (Perkins, 1986).

2.3.5. Stopped-Flow Measurements

Stopped-flow experiments were carried out at 20°C using 2′(3′)-O-N-methylanthraniloyl analogs of GTP and GDP (Jameson and Eccleston, 1997) to study the rates of substrate and product binding and release. The buffer was the same as that used for the ultracentrifugation experiments (see above) and the samples were excited at 280 nm, taking advantage of energy transfer from excited tryptophans to the mant moiety, to increase the signal-to-background ratio (excitation of free mant nucleotides is greatly reduced at this wavelength) and emission at wavelengths greater than 400 nm was observed through a Wratten 47B filter. Measurements were made in a Hi-Tech MX61 stopped-flow fluorometer operated in the single-push mode and data were analyzed using Hi-Tech software.

3. RESULTS AND DISCUSSION

3.1. Analytical Ultracentrifugation

3.1.1. Sedimentation Equilibrium

In order to better understand the connections between dynamin self-association and its GTPase activity, we first looked at the stoichiometry of self-assembly of native dynamin (without any activators). Figure 1 shows various fits to the data for different models, along with the residuals for each fit, using the programs described in Section 2. The models tried were monomer alone (Fig. 1A, assuming

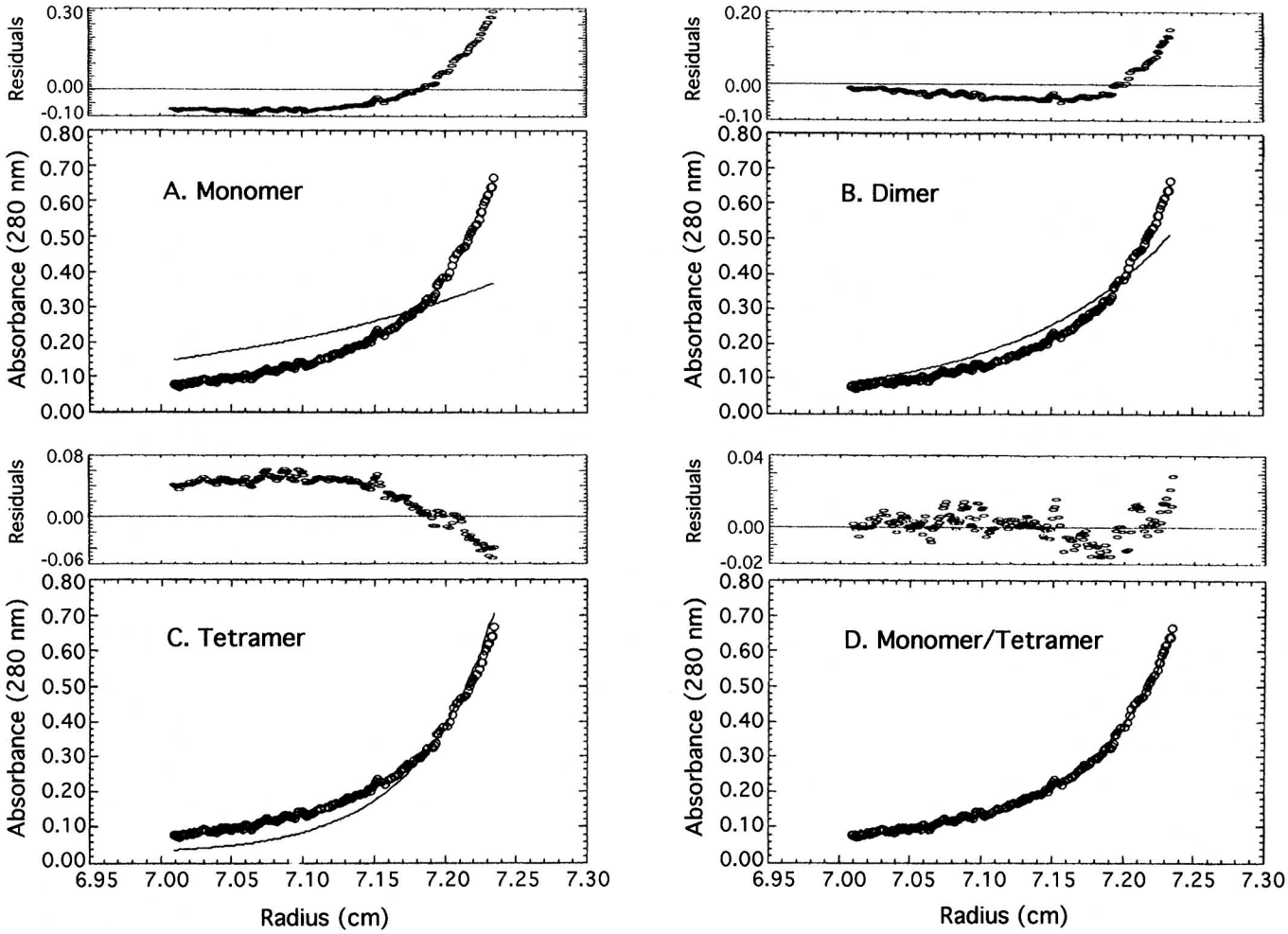

Fig. 1. Sedimentation equilibrium data fit to different models: (A) monomer alone; (B) dimer alone; (C) tetramer alone; (D) monomer/tetramer.

a molecular weight of 100 kDa), dimer alone (Fig. 1B), and tetramer alone (Fig. 1C). These models did not provide good fits to the data, and the residuals displayed a definite, nonrandom pattern. We also tried to fit the data to a single species, but this gave a molecular weight of 285 kDa with similarly poor residuals (data not shown). This molecular weight does not correspond exactly to monomer, dimer, or trimer, and the nonrandom pattern of the residuals clearly indicated that self-association occurred. A monomer–dimer fit (chi^2 for the fit was 1.7×10^{-4}) also displayed nonrandom residuals (data not shown). In contrast, a monomer/tetramer model fit the data very well ($chi^2 = 6.37 \times 10^{-5}$), and displayed a tighter, more random fit to the residuals (Fig. 1D). The monomer/tetramer equilibrium association constant $K_{1,4}$, calculated as described in Section 2, was 1.67×10^{17} M^{-3} with an error of 0.252×10^{17} M^{-3}. Using this equilibrium constant, a plot of the species fraction for both monomer and tetramer relative to the total concentration of monomer in the sample was generated (Fig. 2). From the figure, one can see that at 9×10^{-6} M dynamin monomer, the number of tetramer units is equal to the number of monomer units. Also, from Fig. 2, at about 2×10^{-6} M dynamin monomer, there are as many dynamin molecules in the monomeric form as in the tetrameric form, on a mole:mole basis.

The monomer/tetramer model calculates a fit and an equilibrium constant $K_{1,4}$ for four monomers forming one tetramer, regardless of whether intermediate states (dimers or trimers) are present. We also tried a monomer/dimer/tetramer fit to our data (not shown). The residuals, the chi^2 value, and $K_{1,4}$ for the monomer/ dimer/tetramer fit were the same as for the monomer/ tetramer fit, so there was no demonstrable improvement using this model. The

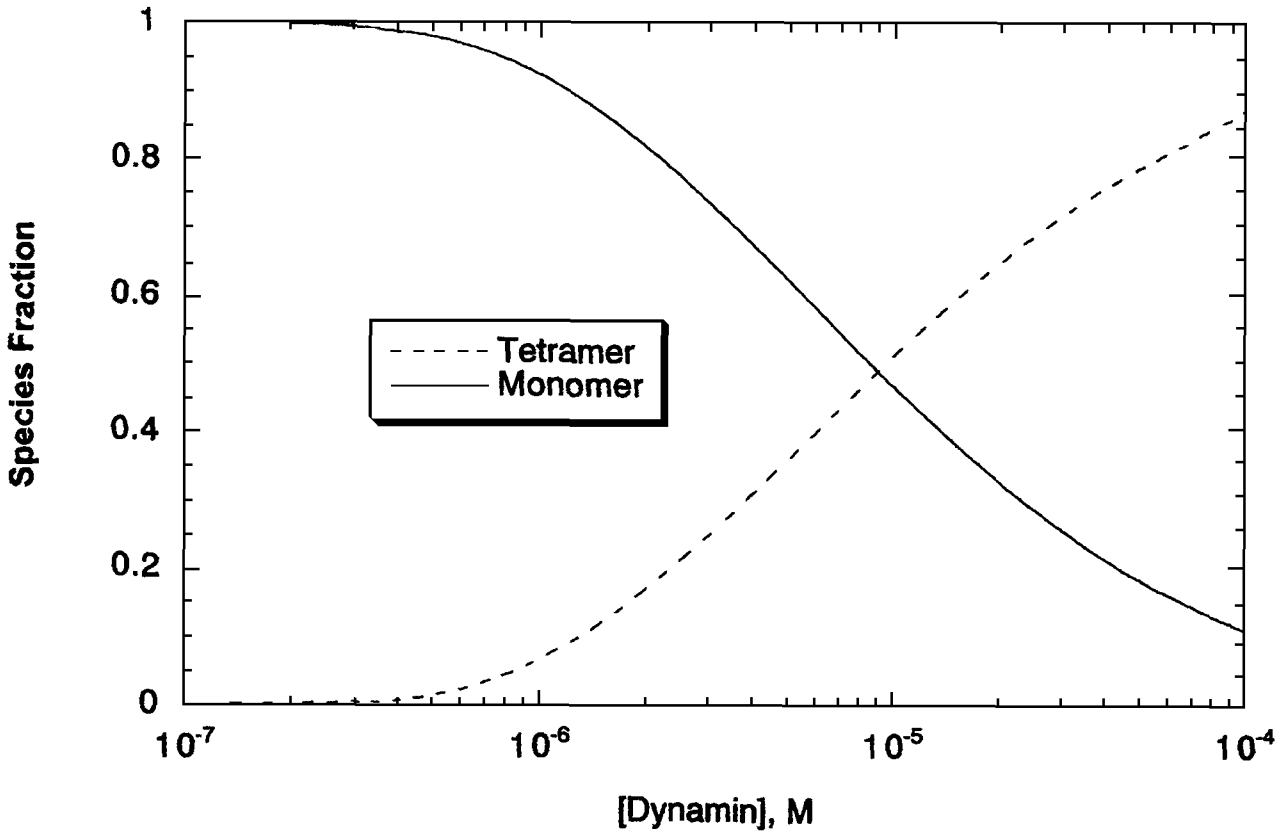

Fig. 2. Species plot for bovine dynamin I assuming the monomer/tetramer model and an equilibrium constant of 1.67×10^{17} M^{-3}.

monomer/dimer equilibrium association constant $K_{1,2}$ was 1.4×10^3 M^{-1}. The small size of $K_{1,2}$ relative to $K_{1,4}$ indicates that very little dimer is present in solution relative to the amount of monomer and tetramer. Thus the dynamin I self-association equilibrium is well described by a monomer/tetramer model.

3.1.2. Sedimentation Velocity

Sedimentation velocity experiments confirmed that dynamin can oligomerize. A plot of the $\ln(r)$ vs. $\omega^2 t$, where the variable r is the position of the equivalent boundary as calculated by the second-moment method, is shown in Fig. 3. The slope of this curve gives the weight-averaged sedimentation coefficient 9.51 S (correlation coefficient = 0.998). Also, the data were analyzed according to the $g(s^*)$ method (see Section 2), which gives an apparent sedimentation coefficient distribution for the sample (Fig. 4). According to this method, the weight-average sedimentation coefficient is 9.54 S, in excellent agreement with the value obtained by the second-moment method.

Using the sedimentation coefficient of 9.5 S, and assuming a population of all monomers, all dimers, or all tetramers, frictional coefficients, the radii of equivalent spheres for a given frictional coefficient, and the minimum radii of a sphere for a protein of a given molecular weight were calculated (Table I). Since R/R_{min} must always be greater than or equal to one, it is evident that dynamin cannot be exclusively in the monomeric state, but that higher order structures must exist in solution. Also, from the $g(s^*)$ plot in Fig. 4, we can see that the peak of the $g(s^*)$ curve is at 8.1 S. The curve is asymmetrical, since the weight-averaged sedimentation coefficient is 9.54 S, which is significantly different than the peak S value. Such an asymmetry in the sedimentation coefficient distribution function is also consistent with self-association.

3.2. Kinetic Analysis of the Interactions of Mant-Nucleotides with Dynamin

The interaction of mant-nucleotides with dynamin was investigated by stopped-flow fluorescence measure-

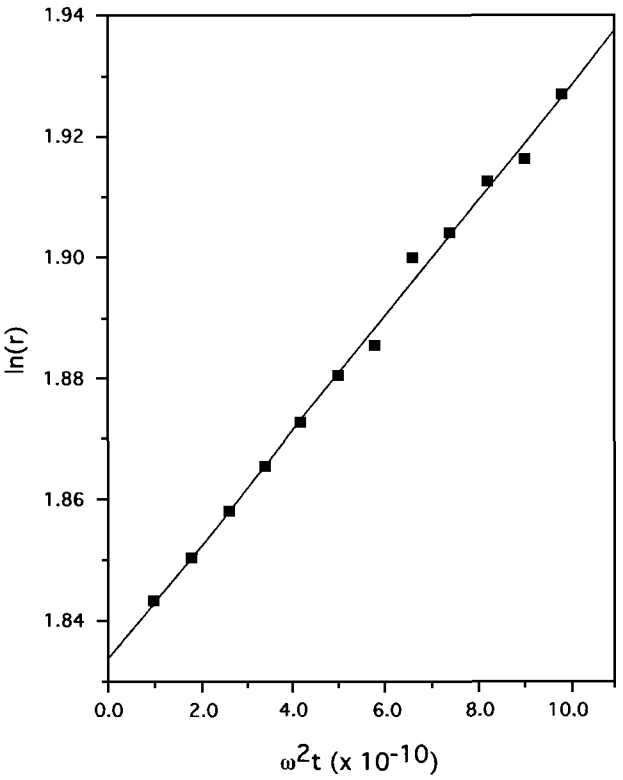

Fig. 3. Secondary plot of sedimentation velocity data for determination of the sedimentation coefficient.

ments. On mixing 1 μM dynamin with 10 μM mantGTP, there was an increase in fluorescence intensity which could be fitted to a single exponential giving a rate constant of 9.5 s^{-1} (Fig. 5A). The experiment was repeated over the concentration range of 5–60 μM mantGTP. There was a linear dependence of the observed rate constant on [mantGTP] (Fig. 5B). If binding is assumed to be a single-step process, then

$$k_{obs} = k_1[\text{mantGTP}] + k_{-1} \quad (5)$$

Therefore, a plot of k_{obs} against [mantGTP] gives a slope of k_1 and an intercept of k_{-1}. The slope of this line gave a second-order association rate constant of 7.0×10^5 M^{-1} s^{-1}. The intercept of this plot gave a value for the dissociation rate constant of 1.8 s^{-1}, but this value could not be defined accurately. Therefore the dissociation rate constant was measured by a displacement reaction. A solution containing 2 μM dynamin and 4 μM mantGTP was mixed with a solution of 200 μM GTP. A decrease in fluorescence intensity occurred which could be fitted to a single exponential giving a dissociation rate constant of 2.1 s^{-1}. However, there was a systematic deviation of the fit from the data, and a better fit was obtained to a double-exponential model giving rate constants of 5.8 and 1.1 s^{-1}. It is not yet known whether the two exponentials arise from dissociation of mantGTP from different oligomeric species of dynamin, or from two different conformational states of dynamin, or from the presence of the 2′ and 3′ derivatized isomers of mantGTP (Jameson and Eccleston, 1997). From the relationships $K_D = k_{diss}/k_{ass}$, and using the value of the single-exponential fit to the displacement experiment, a K_D value of 2.5 μM is obtained for the binding of mantGTP to dynamin.

Similar binding experiments were performed with dynamin and mantGDP. However, mantGDP bound significantly weaker than mantGTP. This resulted in the need for higher concentrations of mantGDP being required to form observable concentrations of dynamin: mantGDP complex, but at these concentrations the association reaction became too fast to measure. The displacement of mantGDP from dynamin could be observed. On mixing a solution of 2 μM dynamin and 5 μM mantGDP with a solution of 200 μM GTP, an exponential decrease in fluorescence occurred with a first-order rate constant of 93 s^{-1} (Fig. 5D). If the difference in the K_D for mantGTP and mantGDP binding to dynamin is governed by only the dissociation rate constants, then mantGDP binds approximately 40-fold more weakly than mantGTP.

3.3. Characterization of Cooperative Dynamin–Dynamin Interaction on a Microtubule Lattice

Tuma and Collins (1994) demonstrated that microtubule-stimulated GTPase activity of dynamin increases as a function of dynamin concentration, suggesting that dynamin self-association is a key feature in the regulation of its enzymatic activity. We extended their work in an effort to explain the reported biphasic activation of dynamin GTPase activity by microtubules and to further characterize the dynamin–dynamin interaction. Figure 6A confirms the original observation of Tuma and Collins (1994) that GTPase activity depends on dynamin concentration, but also shows that the activation profiles are dependent on the fixed microtubule concentration used for each activation curve. At higher microtubule concentrations, more dynamin is required to achieve maximal enzymatic activity. The simplest explanation for this result is that dynamin can distribute among more potential binding sites at higher microtubule concentrations, thereby decreasing the number of contiguous dynamin molecules expressing high GTPase activity. Consequently, when dynamin GTPase

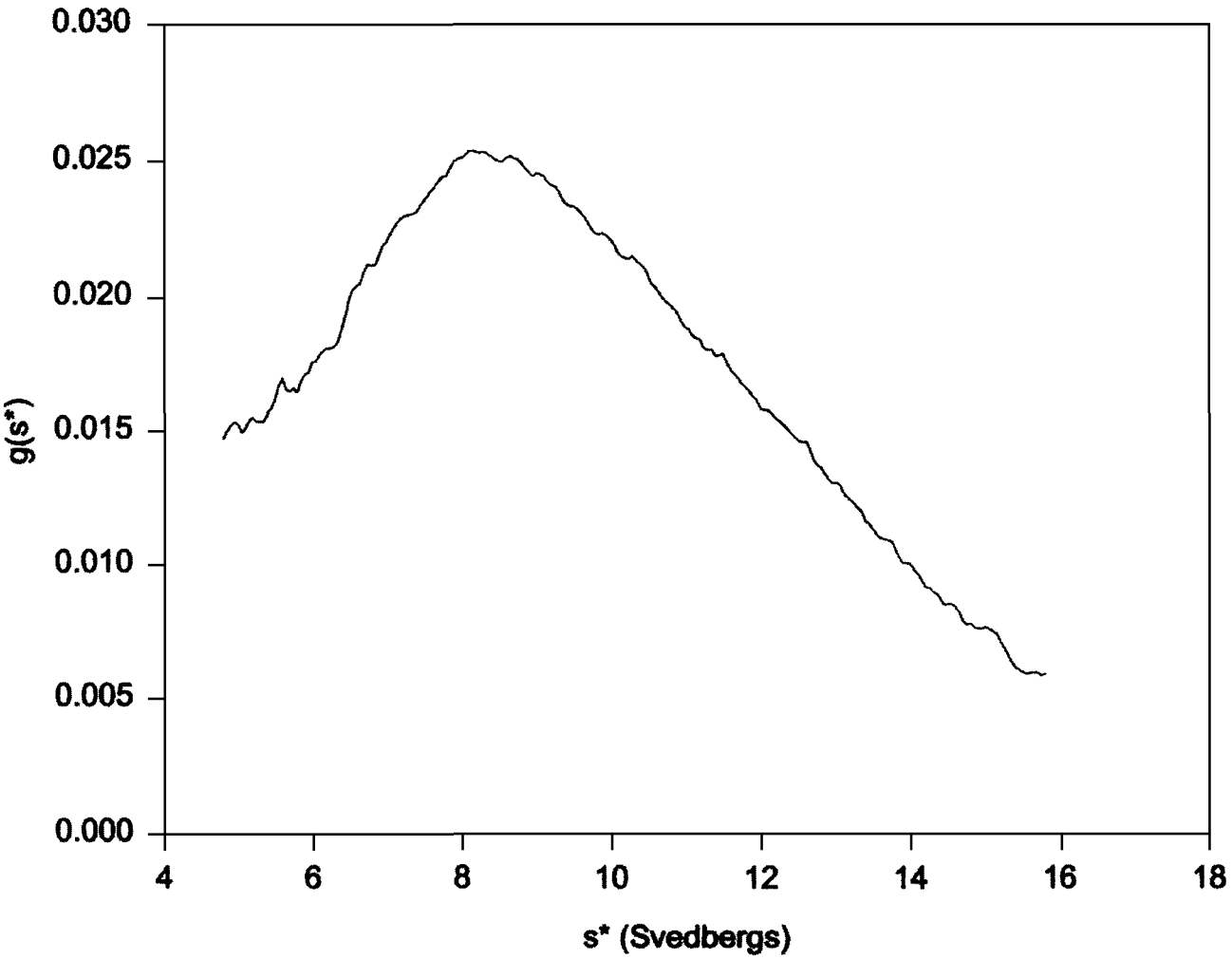

Fig. 4. Sedimentation coefficient distribution analysis.

activity is measured as a function of microtubule concentration (at a fixed dynamin concentration), the characteristic biphasic profiles (Tuma and Collins, 1994; Lin *et al.*, 1997) are obtained. As expected, the downward phase of these activation profiles occurs at high microtubule concentrations if higher dynamin concentrations are used in the assays (Fig. 6B). Although active dynamin oligomers can apparently be prevented from forming at high microtubule concentrations (at dynamin: tubulin monomer ratios of about 1:20 or greater), there is nevertheless a strong tendency for dynamin molecules to self-assemble on the microtubule scaffold. Figure 7 contrasts the actual GTPase activities of microtubule-bound dynamin with the predicted activities if the same amounts of dynamin were randomly distributed on the microtubule lattice. In calculating the theoretical activation curve for random distribution, the assumptions were made that each tubulin monomer can bind a dynamin molecule [for support of this assumption, see Maeda *et al.*, (1992)] and that all contiguous dynamin molecules express maximal activity, whereas separated dynamin

Table I. Calculated Values for the Frictional Ratio of Dynamin I[a]

M	f	R	R_{min}	f/f_{min}
100,000	4.72×10^{-8}	2.5×10^{-7}	3.07×10^{-7}	0.81
200,000	9.44×10^{-8}	5×10^{-7}	3.86×10^{-7}	1.3
400,000	1.88×10^{-7}	1×10^{-6}	4.87×10^{-7}	2.1

[a] These values were calculated using the relations given in Section 2 and assuming a sedimentation coefficient of 9.5 S. M, Molecular weight; f, frictional coefficient in g/sec, calculated assuming $\eta = 0.01$P; R, radius (in cm) of an equivalent sphere with frictional coefficient f; R_{min}, minimum radius (in cm) of a spherical unhydrated protein with molecular weight M; f/f_{min}, frictional ratio, where f_{min} is calculated from $f_{min} = 6\pi\eta R_{min}$.

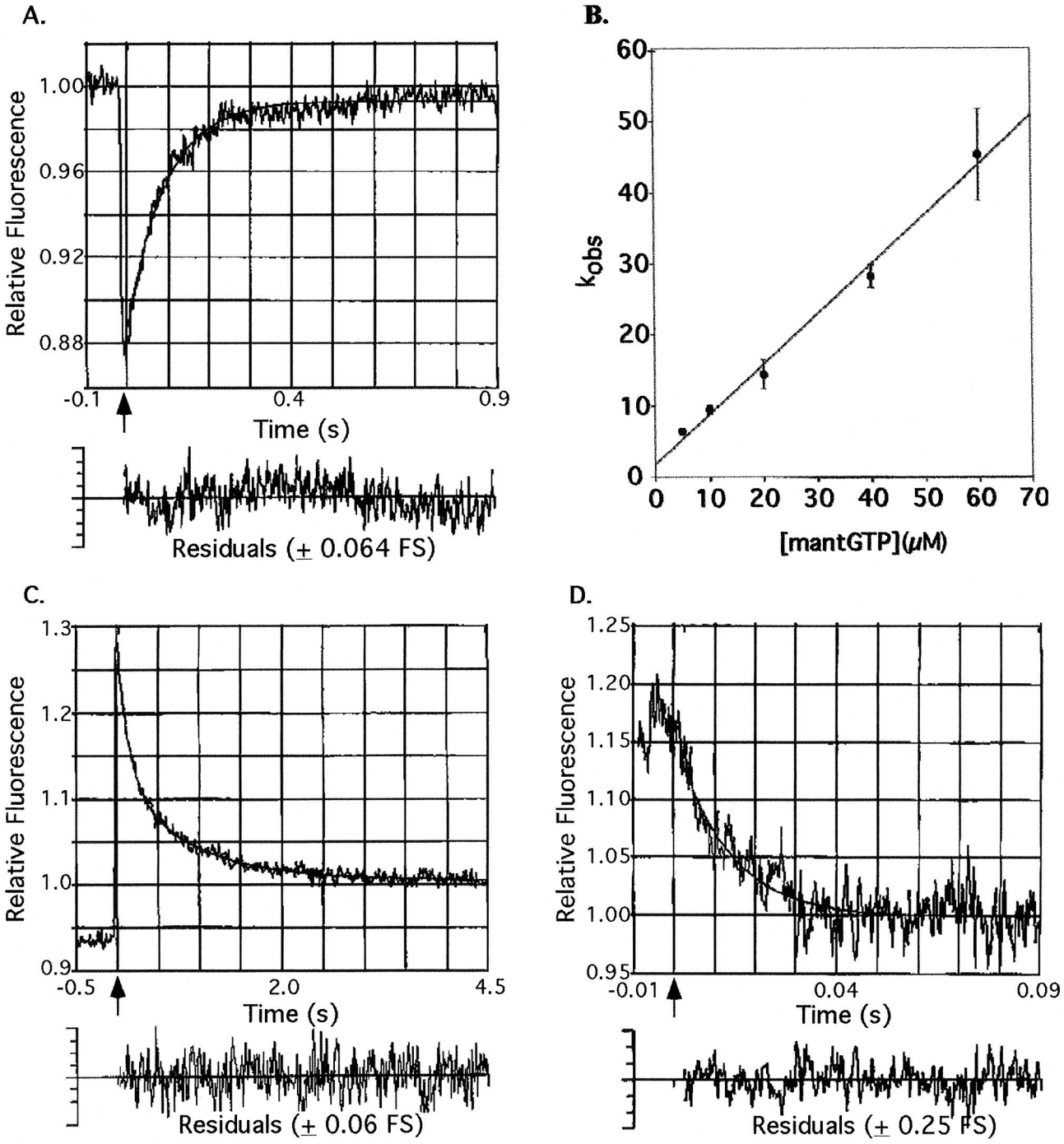

Fig. 5. Stopped-flow fluorescence records of the interaction of mantGTP and mantGDP with dynamin. (A) One syringe contained 1 μM dynamin and the other 10 μM mantGTP. The fitted line is a single exponential with a rate constant of 9.5 s^{-1}. (B) Data from panel A were fitted to single exponentials and the observed rate constants fitted to [mantGTP]. The straight line has a slope of 7.0×10^5 M^{-1} s^{-1} and an intercept of 1.8 s^{-1}. (C) One syringe contained 2 μM dynamin and 4 μM mantGTP and the other contained 200 μM GTP. The fitted line is to a double exponential with rate constants of 5.8 and 1.1 s^{-1}. (D) One syringe contained 2 μM dynamin and 5 μM mantGDP and the other contained 200 μM GTP. The fitted line is to a single exponential with a rate constant of 93 s^{-1}.

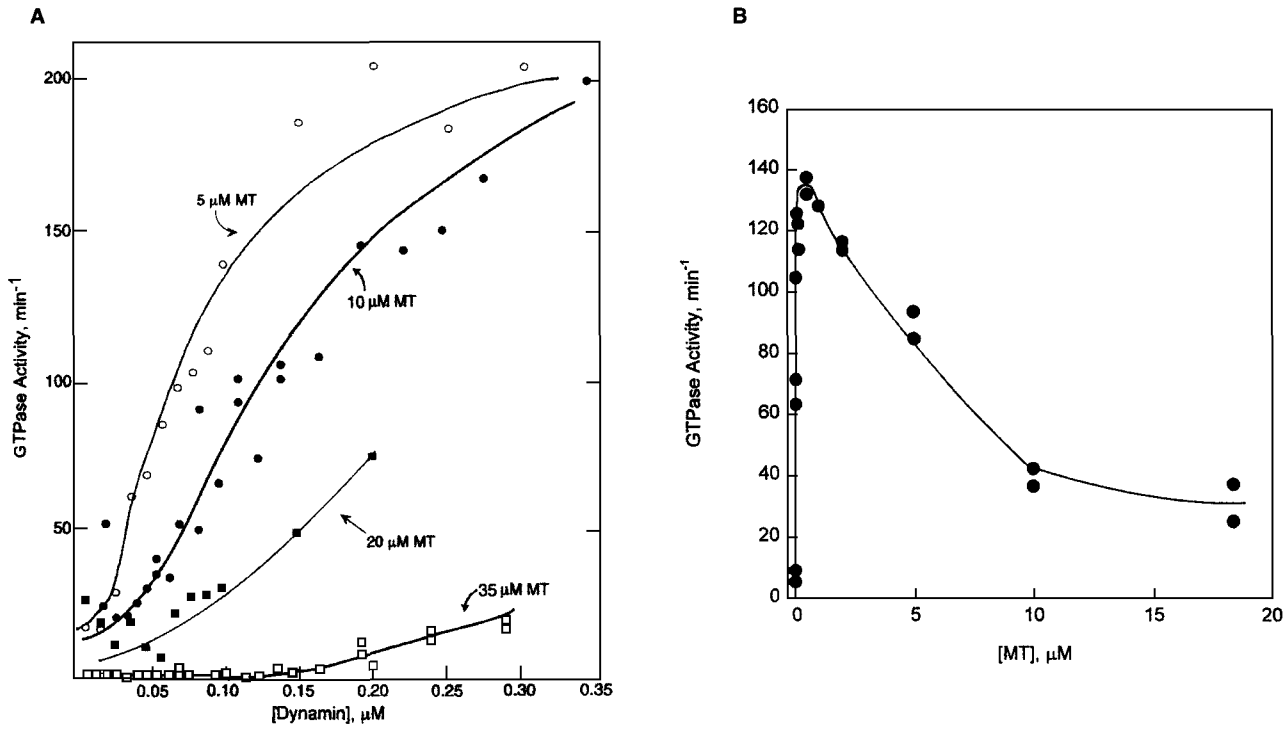

Fig 6. Microtubule-stimulated GTPase activity of dynamin. (A) GTPase activity as a function of dynamin concentration at 5, 10, 20, and 35 μM microtubules. (B) GTPase activity as a function of microtubule concentration at 0.1 μM dynamin. Microtubule concentration expressed in terms of tubulin monomer concentration. Bovine serum albumin (final concentration 0.25 mg/ml) was added due to low concentrations of dynamin in some assays.

molecules are significantly less active. Figure 7 clearly shows that self-association is favored over random distribution. This result is in agreement with our binding Studies (See below, Fig. 8).

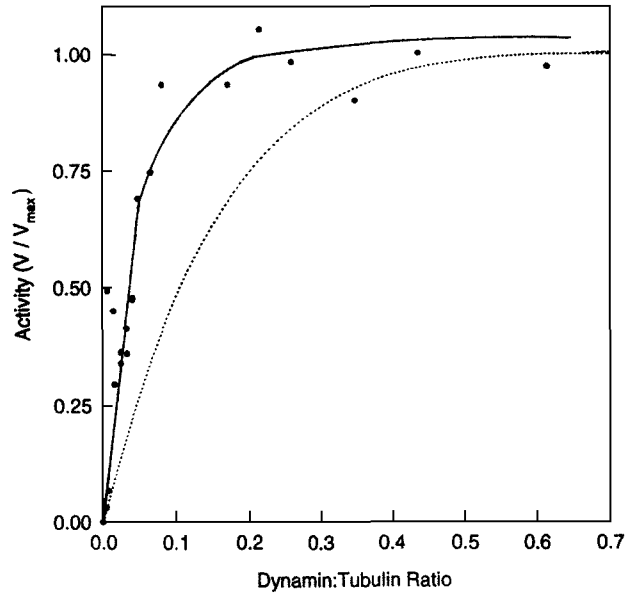

3.4. Dynamin Self-Association Is Insufficient for Maximal GTPase Activation

At low salt concentration (25–50 mM NaCl) dynamin self-assembles into large, sedimentable structures composed of rings and stacks of interconnected rings (Hinshaw and Schmid, 1995). As demonstrated by the pelleting assay shown in Fig. 8A, dynamin aggregates at low ionic strength in a protein concentration-dependent manner, and this aggregation is inhibited at 40 mM NaCl. However, the basal GTPase activity was invariant over a broad range of dynamin concentrations up to 5 μM,

Fig. 7. GTPase activity of dynamin as a function of dynamin–tubulin ratio. The dashed curve represents the predicted outcome for random (noncooperative) distribution of dynamin on the microtubule lattice. The assumption made in generating this theoretical profile is that all contiguous dynamin molecules express maximal activity, whereas isolated dynamins express no enzymatic activity. Therefore, the curve is the probability that, at each dynamin–tubulin ratio, a dynamin molecule will be situated next to another dynamin molecule. The solid line is a visual fit through the actual data points. Note that the GTPase activities rise far more steeply than would be expected for a random distribution, demonstrating the strongly cooperative dynamin–dynamin interactions occurring along the microtubule.

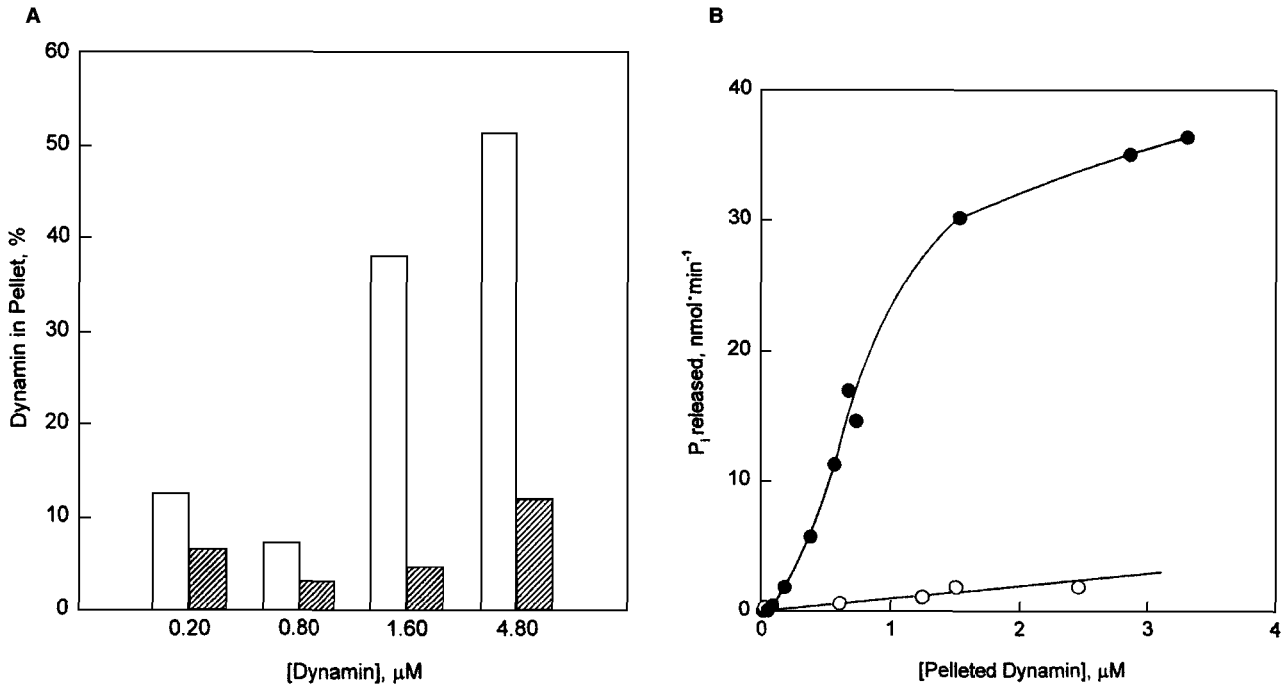

Fig. 8. Correlation of GTPase activity with self-association of dynamin. (A) Sedimentation of dynamin in the absence (empty bars) or presence (striped bars) of 40 mM NaCl. (B) GTPase activity in the absence (○) or presence (●) of microtubules versus the amount of sedimented dynamin.

wherein approximately 50% of the enzyme is in the aggregated state under assay conditions (Fig. 8B). In the presence of microtubules, the GTPase activities of these samples were stimulated to levels of approximately 200 min^{-1}. The lack of activity of dynamin aggregates alone indicates that mere proximity of dynamin molecules cannot adequately explain the high catalytic turnover numbers observed when the enzyme is bound to microtubules. Instead, it suggests that dynamin molecules must be properly oriented in order to express high GTPase activity, and that microtubules are able to induce this orientation.

3.5. Effect of Salt on Dynamin GTPase Activity

Microtubule-stimulated GTPase activity of dynamin is strongly inhibited by relatively low concentrations of salt [less than 50 mM NaCl (Tuma *et al.*, 1993; Warnock and Schmid, 1996; Lin *et al.*, 1997)], whereas activation of GTPase by Grb2 is unaffected even at concentrations as high as 200 mM (Lin *et al.*, 1997). This result (shown again in Fig. 9) reflects the ionic nature of the microtubule–dynamin interaction and supports the view that SH3 domain interactions (such as those involving Grb2) are dominated by nonionic effects. However, direct binding studies revealed that the dramatic reduction in microtubule-stimulated activity could not be explained solely by a weakened affinity of dynamin for microtubules. NaCl (40 mM) reduces the amount of dynamin bound to microtubules by only 20%, but abolishes enzymatic activity. These data suggest that salt inhibits both dynamin–microtubule and dynamin–dynamin interactions. The latter possibility is represented schematically in Fig. 10. Consequently, the GTPase activities of microtubule-bound dynamin are reduced by NaCl (Fig. 11). In contrast, GTPase activity was unaffected by nonionic detergent (data not shown).

Results obtained from pelleting experiments are presented in the form of Scatchard plots in Fig. 11B. As expected, salt not only weakens the affinity of dynamin for microtubules, but also reduces the cooperative nature of the binding, presumably due to a weakening of the dynamin–dynamin interaction.

4. CONCLUSION

The important role of reversible dynamin oligomerization in the process of membrane internalization is now widely accepted. Tuma and Collins (1994) first

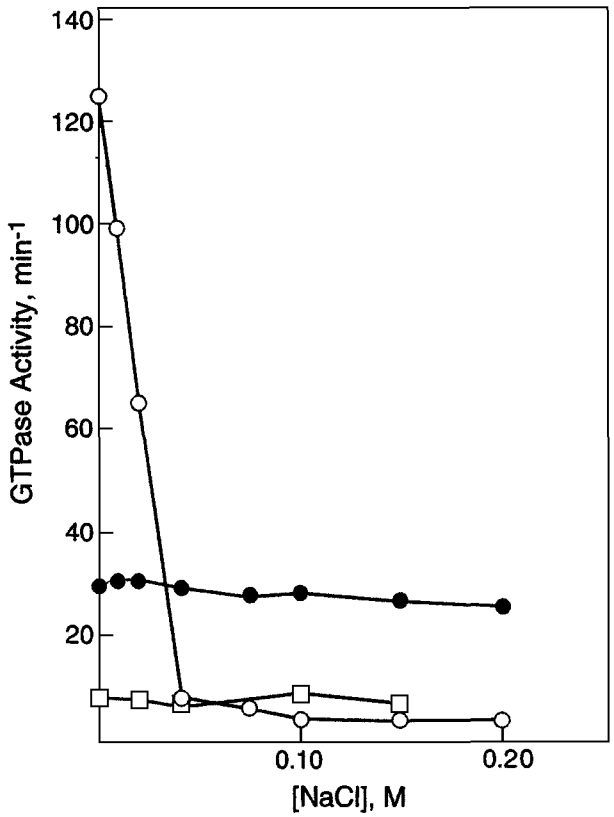

Fig. 9. Effect of NaCl on the GTPase activity of dynamin alone (□), or in the presence of Grb2 (●) or microtubules (○). Concentration of dynamin, microtubules, or Grb2 is 0.2, 3, or 2 μM, respectively.

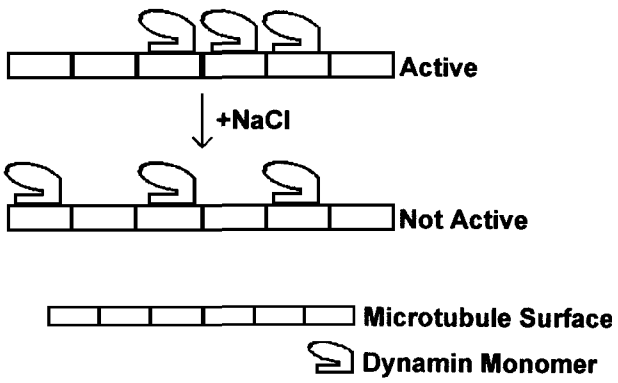

Fig. 10. Schematic illustration of the distribution of dynamin on microtubules in the presence and absence of salt.

showed that GTP hydrolysis is coupled to dynamin self-association which occurs in a cooperative manner on the surfaces of microtubules and liposomes. The cooperative nature of the dynamin–dynamin interaction is reduced by salt, demonstrating the ionic basis of this interaction. We present data indicating that close proximity of dynamin molecules is not sufficient for expressing high GTPase activity. For example, Grb2 cross-links dynamin molecules, but simultaneous stimulation of GTPase activity is much lower than that obtained with microtubules [44 min^{-1} versus 200 min^{-1} (Lin *et al.*, 1997)]. Our results agree with those of Warnock *et al.* (1995) in which an antibody (Hudy2) against an epitope in the C-terminal region of dynamin cross-links the enzyme and can also stimulate GTPase activity to a similar level as Grb2. Taken together, the results show the importance of proper dynamin conformation or orientation for expression of its enzymatic activity. In this paper, we also describe nucleotide-binding and oligomerization properties of bovine brain dynamin I in the absence of GTPase-activating molecules. These experiments were carried out at 0.3 M NaCl, a salt concentration which inhibits the formation of higher order aggregates such as rings and coils which form under low-salt conditions (Hinshaw and Schmid, 1995) or at physiological ionic strength in the presence of GTP (Carr and Hinshaw, 1997). A characteristic of most guanine nucleotide-binding proteins involved in signaling, including the heterotrimeric G proteins and Ras-like proteins, is their high affinity for GTP and GDP. For example, $G_s\alpha$ and Ras bind GDP with dissociation constants in the nanomolar range (Higashijima *et al.*, 1987; John *et al.*, 1990; Neal *et al.*, 1990). Therefore, guanine nucleotide releasing or exchange factors (GRFs or GEFs) are required for efficient cycling through the GTPase reaction during signal transduction. As demonstrated by our stopped-flow analysis, dynamin binds fluorescent guanine nucleotide analogs relatively weakly (K_D in the micromolar range). In this respect dynamin is more similar to the force-generating ATPases (e.g., myosin, dynein, and kinesin) than to the signaling G-proteins, consistent with a role as a membrane "pinchase" rather than a molecular switch.

Recently, Muhlberg et al. (1997) concluded, on the basis of sedimentation equilibrium experiments under high-salt conditions (400 mM potassium phosphate, pH 7.0), that dynamin is a tetramer. Our sedimentation equilibrium results, however, demonstrate that dynamin I exists in a monomer–tetramer equilibrium in high salt (0.3 M NaCl). Our sedimentation velocity data also confirm that multiple oligomeric states of dynamin are present under these conditions. These results raise the possibility of an additional mode of dynamin regulation in cells, i.e., control of its assembly into tetramers, which presumably are the building blocks for the rings and coils that form around the necks of budding endosomes.

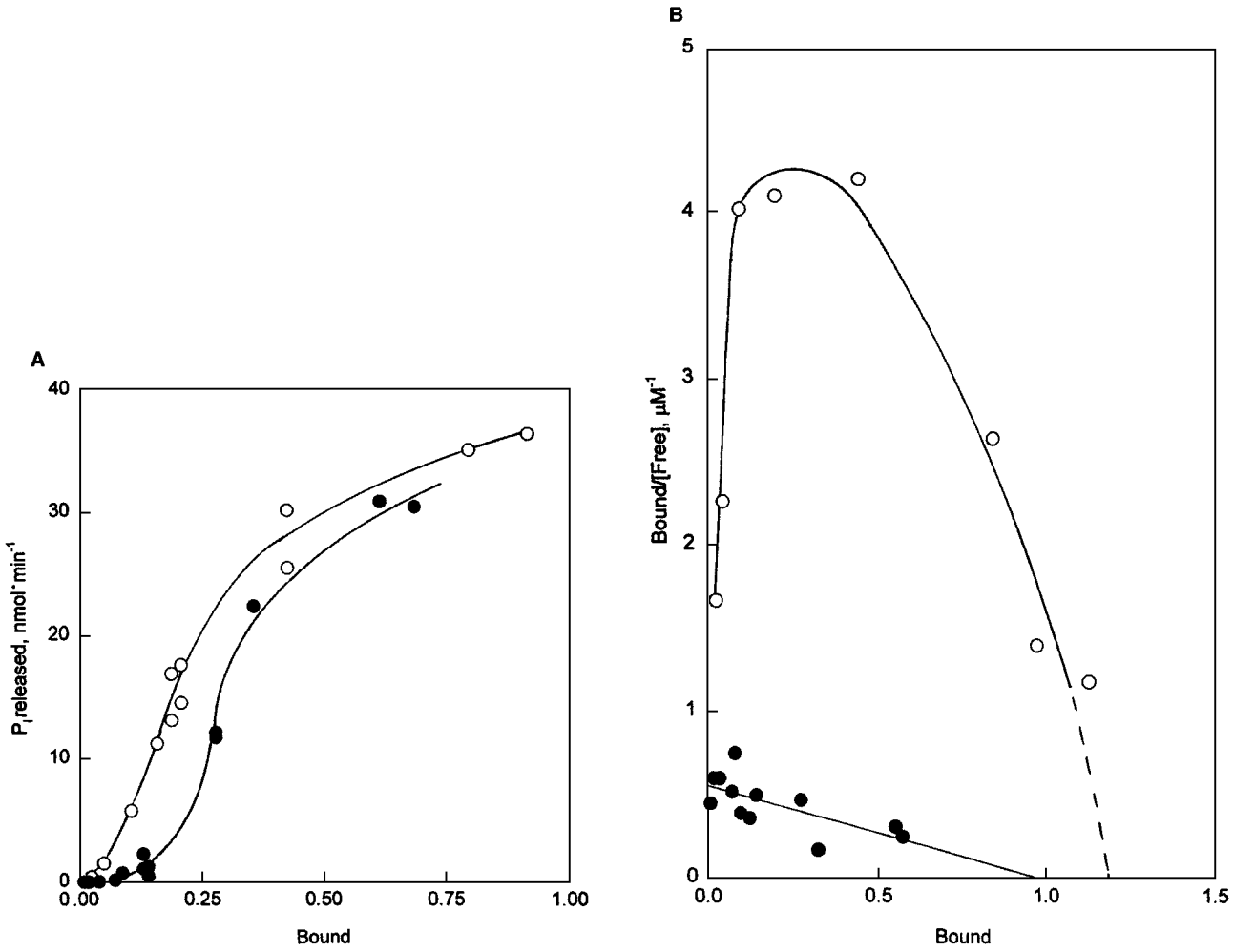

Fig. 11. Effect of 40 mM NaCl on dynamin–microtubule interaction. (A) GTPase activity of microtubule-bound dynamin in the presence (●) or absence (○) of salt. (B) Scatchard plots of microtubule-dynamin binding in the presence (●) or absence (○) of salt. Activity is plotted as a function of mol dynamin bound per mol tubulin monomer. The microtubule concentration was 3.4 μM, and the dynamin concentration ranged from 0.05 to 4 μM.

ACKNOWLEDGMENT

We thank Heather Brogan for excellent technical assistance.

This research was supported by National Institutes of Health Grant GM555620 (J.P.A.), American Heart Association, Texas Affiliate Grant 97G-111 (B.B.), the University Research Council of the University of Hawaii (D.M.J.), American Heart Association Grant 9950020N (D.M.J.), and by the Medical Research Council, U.K. (J.F.E.).

REFERENCES

Ando, A., Yonezawa, K., Gout, I., Nakata, T., Ueda, H., Hara, K., Kitamira, Y., Takenawa, T., Hirokawa, N., Waterfield, M. D., and Kasuga, M. (1994). *EMBO J.* **13**, 3033–3038.

Bradford, M. M. (1976). *Anal. Biochem.* **72**, 248–254.

Carr, J. F., and Hinshaw, J. E. (1997). *J. Biol. Chem.* **272**, 28030–28035.

Chen, M. S., Obar, R. A., Schroeder, C. C., Austin, T. W., Poodry, C. A. Wadsworth, S. C., and Vallee, R. B. (1991). *Nature* **351**, 583–586.

Cohn, E. J., and Edsall, J. T. (1943). *Proteins, Amino Acids and Peptides as Ions and Dipolar Ions,* Reinhold, New York (reprinted 1965, Hafner, New York).

Cook, T. A., Urruita, R., and McNiven, M. A. (1994). *Proc. Natl. Acad. Sci. USA* **91**, 644–648.

Damke, H. Baba, T. Warnock, D. E., and Schmid, S. L. (1994). *J. Cell Biol.* **127**, 915–934.

David, C., McPherson, P. S., Mundigl, O., and De Camilli, P. (1996). *Proc. Natl. Acad. Sci. USA* **93**, 331–335.

De Camilli, P. (1995). *FEBS Lett.* **369**, 3–12.

Earnest, S. Khokhlatchev, A., Albanesi, J. P., and Barylko, B. (1996). *FEBS Lett.* **396**, 62–66.

Gout, I., Dhand, R., Hiles, I. D., Fry, M. J., Panayotou, G., Das, P., Truong, O., Totty, N. F., Hsuan, J., Booker, G. W., Campbell, I. D., and Waterfield, M. D. (1993). *Cell* **75**, 25–36.

Hensley, P. (1996). *Structure* **4**, 367–373.

Herskovits, J. S., Burgess, C. C., Obar, R. A., and Vallee, R. B. (1993*a*). *J. Cell Biol.* **122**, 565–578.
Herskovits, J. S., Shpetner, H. S., Burgess, C. C., and Vallee, R. B. (1993*b*). *Proc. Natl. Acad. Sci. USA* **90**, 11468–11472.
Higashijima, T., Ferguson, K. M., Sternweis, P. C., Smigel, M. D., and Gilman, A. G. (1987). *J. Biol. Chem.* **262**, 762–766.
Hinshaw, J. E., and Schmid, S. L. (1995). *Nature* **374**, 190–192.
Jameson, D. M., and Eccleston, J. F. (1997). *Meth. Enzymol.* **278**, 363–390.
Jin, M., and Snider, M. D. (1993). *J. Biol. Chem.* **268**, 18390–18397.
John, J., Sohmen, R., Feuersten, J., Linke, R., Wittinghofer, A., and Goody, R. S. (1990). *Biochemistry* **29**, 6058–6065.
Kelly, W. G., Passanti, A., Woods, J. W., Daiss, J. L., and Roth, T. F. (1993). *J. Cell Biol.* **97**, 1191–1199.
Korn, E. D., Collins, J. H., and Maruta, H. (1982). *Meth. Enzymol.* **85**, 357–363.
Laemmli, U. K. (1970). *Nature* **227**, 680–685.
Lin, H. C., Barylko, B. Achiriloaie, M., and Albanesi, J. P. (1997). *J. Biol. Chem.* **272**, 25999–26004.
Maeda, K., Nakata, T., Noda, Y., Sato-Yoshitake, R., and Hirokawa, N. (1992). *Mol. Biol. Cell* **3**, 1181–1194.
Matsudaira, P. T., and Burgess, D. R. (1978). *Anal. Biochem.* **87**, 386–396.
McNiven, M. A. (1998). *Cell* **94**, 151–154.
Miki, H., Miura, K., Matuoka, K., Nakata, T., Hirokawa, N., Orita, S., Kaibuchi, K., Takai, Y., and Takenawa, T. (1994). *J. Biol. Chem.* **269**, 5489–5492.
Muhlberg, A. B. Warnock, D. E., and Schmid, S. L. (1997). *EMBO J.* **16**, 6676–6683.
Nakata, T., Takemura, T., and Hirokawa, N. (1993). *J. Cell Sci.* **105**, 1–5.
Neal, S. E., Eccleston, J. F., and Webb, M. R. (1990). *Proc. Natl. Acad. Sci USA* **87**, 3562–3565.
Obar, R. A., Collins, C. A., Hammerback, J. A., Shpetner, H. S., and Vallee, R. B. (1990). *Nature* **347**, 256–261.
Perkins, S. J. (1986). *Eur. J. Biochem.* **157**, 169–180.
Roos, J., and Kelly, R. B. (1997). *Trends Cell Biol.* **7**, 257–258.
Salim, K., Bottomley, M. J., Querfurth, E., Zvelebil, M. J., Gout, I., Scaife, R., Margolis, R. L., Gigg, R., Smith, C. I. E., Driscoll, P. C., Waterfield, M. D., and Panayotou, G. (1996). *EMBO J.* **15**, 6241–6250.
Scaife, R., and Margolis, R. L. (1990). *J. Cell Biol.* **111**, 3023–3033.
Scaife, R., Gout, I. Waterfield, M. D., and Margolis, R. L. (1994). *EMBO J.* **13**, 3033–3038.
Seedorf, K., Kostka, G., Lammers, R., Bashkin, P., Daly, R., Burgess, W. H., van der Bliek, A. M., Schlessingers, J., and Ullrich, A. (1994). *J. Biol. Chem.* **269**, 16009–16014.
Shpetner, H. S., and Vallee, R. B. (1992). *Nature* **355**, 733–735.
Sontag, J.-M., Fyske, E. M., Ushkaryov, Y., Liu, J.-P., Robinson, P. J., and Sudhof, T. C. (1994). *J. Biol. Chem.* **269**, 4547–4554.
Stafford, W. F. (1992). *Anal. Biochem.* **203**, 295–301.
Stafford, W. F. (1994). *Meth. Enzymol.* **240**, 478–501.
Sweitzer, S. M., and Hinshaw, J. E. (1998). *Cell* **93**, 1021–1029.
Takei, K., McPherson, P. S., Schmid, S. L., and De Camilli, P. (1995). *Nature* **374**, 186–190.
Takei, K., Haucke, V., Slepnev, V., Farsad, K., Salazar, M., Chen, H., and De Camilli, P. (1998). *Cell* **94**, 131–141.
Tuma, P. L., and Collins, C. A. (1994). *J. Biol. Chem.* **269**, 30842–30847.
Tuma, P. L., Stackniak, M. C., and Collins, C. A. (1993). *J. Biol. Chem.* **268**, 17240–17246.
Urrutia, R., Henly, J. R., Cook, T., and McNiven, M. A. (1997). *Proc. Natl. Acad. Sci. USA* **94**, 377–384.
Vallee, R. B., and Okamoto, P. M. (1995). *Trends Cell Biol.* **5**, 43–47.
Van der Bliek, A. M., and Meyerowitz, E. M. (1991). *Nature* **351**, 411–414.
Van der Bliek, A. M., Redelmeiser, T. E., Damke, H., Tisdale, E. J., Meyerowitz, E. M., and Schmid, S. L. (1993). *J. Cell Biol.* **12**, 553–563.
Wang, L.-H., Sudhof, T. C., and Anderson, R. G. W. (1995). *J. Biol. Chem.* **270**, 10079–10083.
Warnock, D. E., and Schmid, S. L. (1996). *BioEssays* **18**, 885–893.
Warnock, D. E., Terlecky, L. J., and Schmid, S. L. (1995). *EMBO J.* **14**, 1322–1328.
Williams, R. C., and Lee, J. C. (1982). *Meth. Enzymol.* **85**, 376–385.